



Knockdown of CYP24A1 Aggravates $1\alpha,25(\text{OH})_2\text{D}_3$ -Inhibited Migration and Invasion of Mouse Ovarian Epithelial Cells by Suppressing EMT

Ping Wang^{1,2†}, Jiming Xu^{1†}, Weijing You^{1†}, Yongfeng Hou³, Shuiliang Wang², Yujie Ma², Jianming Tan², Zengli Zhang¹, Wentao Hu^{4*} and Bingyan Li^{1,4*}

OPEN ACCESS

Edited by:

Jiang-Jiang Qin,
Zhejiang Chinese Medical
University, China

Reviewed by:

Dimitar Avtanski,
Northwell Health, United States
Qi Zeng,
Xidian University, China

*Correspondence:

Wentao Hu
wthu@suda.edu.cn
Bingyan Li
bingyanli@suda.edu.cn

[†]These authors have contributed
equally to this work

Specialty section:

This article was submitted to
Pharmacology of Anti-Cancer Drugs,
a section of the journal
Frontiers in Oncology

Received: 16 April 2020

Accepted: 18 June 2020

Published: 29 July 2020

Citation:

Wang P, Xu J, You W, Hou Y, Wang S,
Ma Y, Tan J, Zhang Z, Hu W and Li B
(2020) Knockdown of CYP24A1
Aggravates $1\alpha,25(\text{OH})_2\text{D}_3$ -Inhibited
Migration and Invasion of Mouse
Ovarian Epithelial Cells by
Suppressing EMT.
Front. Oncol. 10:1258.
doi: 10.3389/fonc.2020.01258

¹ Department of Nutrition and Food Hygiene, School of Public Health, Soochow University, Suzhou, China, ² Fujian Key Laboratory of Transplant Biology, 900 Hospital of the Joint Logistics Team, Fuzhou, China, ³ State Key Laboratory of Cardiovascular Disease, National Center for Cardiovascular Diseases, Fuwai Hospital, Chinese Academy of Medical Sciences and Peking Union Medical College, Beijing, China, ⁴ State Key Laboratory of Radiation Medicine and Protection, Collaborative Innovation Center of Radiological Medicine of Jiangsu Higher Education Institutions, School of Radiation Medicine and Protection, Soochow University, Suzhou, China

Epithelial-mesenchymal transition (EMT) bestows cancer cells with motile and invasive properties. But for ovarian tissues, EMT plays a physiological role in the postovulatory repair of ovary surface epithelial (OSE) cells. Accumulating data indicated that $1\alpha,25(\text{OH})_2\text{D}_3$ decreased both the migration and invasion of various cancer cells by suppressing EMT. However, it remains unclear whether $1\alpha,25(\text{OH})_2\text{D}_3$ inhibits the process of EMT during different stages of oncogenic transformation in mouse OSE (MOSE) cells. In present study, a spontaneous malignant transformation model of MOSE cells at three sequential stages (early, intermediate and late) was established *in vitro* first and then subjected to $1\alpha,25(\text{OH})_2\text{D}_3$ treatment to investigate the effect of $1\alpha,25(\text{OH})_2\text{D}_3$ on the oncogenic transformation of MOSE cells. We found that $1\alpha,25(\text{OH})_2\text{D}_3$ significantly reduced the proliferation and invasion of late malignant transformed MOSE (M-L cells) cells by inhibiting EMT both *in vitro* and *in vivo*, but not in intermediate transformed (M-I) cells. Importantly, we found that the levels of CYP24A1 in M-I cells were dramatically higher than that in M-L cells following treatment with $1\alpha,25(\text{OH})_2\text{D}_3$. Furthermore, we demonstrated that, in both M-I and M-L cells with CYP24A1 knockdown, $1\alpha,25(\text{OH})_2\text{D}_3$ suppressed the proliferation and invasion, and reduced the expression of N-cadherin, Vimentin, β -catenin and Snail. In addition, knockdown of CYP24A1 suppressed EMT by increasing E-cadherin while decreasing N-cadherin, Vimentin, β -catenin and Snail. These findings provide support for inhibiting CYP24A1 as a potential approach to activate the vitamin D pathway in the prevention and therapy of ovarian cancer.

Keywords: CYP24A1, $1\alpha,25(\text{OH})_2\text{D}_3$, migration, invasion, epithelial-mesenchymal transition

INTRODUCTION

Epithelial mesenchymal transition (EMT) is a multi-step process by which epithelial cells lose epithelial features and acquire characteristics of mesenchymal cells. The EMT is of great significance to processes involving loss of intercellular adhesion and cell polarity and acquisition of migratory and invasive capacities, such as embryonic development, wound healing, organ fibrosis, etc. Substantial evidence suggest that EMT is abnormally activated during the process of tumor initiation and development as well as in the acquisition of drug resistance (1). In ovarian tissue in particular, EMT plays not only a physiological role in the postovulatory repair of the ovary surface epithelial (OSE) cells, but also a role in the aggressiveness and recurrence of ovarian cancer (2). Ovarian epithelial carcinoma, accounting for more than 90% of all ovarian malignancies, is the most fatal gynecological malignancy due to its strong metastatic ability (3). Key events critical for the migration and invasiveness of epithelial ovarian cancer cells include the invasion of surrounding tissue, the generation of circulating cancer cells, intravasation and survival in the circulation system, the penetration of blood vessels, and the growth at secondary sites (4–6). These cells are endowed with invasion abilities and are able to initiate tumor generation at different sites by undergoing EMT (7). Thus, the development of new therapies able to suppress EMT is therefore needed.

In recent decades, $1\alpha,25$ -dihydroxyvitamin D₃ ($1\alpha,25(\text{OH})_2\text{D}_3$), which is the active form of vitamin D, has been investigated preclinically for its potential in anti-cancer therapy (8, 9). Suboptimal levels of 25 hydroxyvitamin D, the precursor of $1\alpha,25(\text{OH})_2\text{D}_3$, are associated with a poor prognosis in patients with ovarian cancer (9). In addition, results have indicated that $1\alpha,25(\text{OH})_2\text{D}_3$ and its synthetic derivatives inhibit metastasis of many kinds of cancers, including colon, pancreatic, and breast cancers by impeding the progress of an EMT (10–12). We also found that $1\alpha,25(\text{OH})_2\text{D}_3$ suppresses the migration of human ovarian cancer cells by inhibiting EMT (13). However, a meta-analysis did not identify a significant correlation between serum 25, hydroxyvitamin D levels and the risk of ovarian cancer (16), and the efficacy of $1\alpha,25(\text{OH})_2\text{D}_3$ on ovarian cancer has yet to be supported by results from randomized controlled trials (14). Thus, it is important to investigate the mechanisms underlying the anti-cancer effects of $1\alpha,25(\text{OH})_2\text{D}_3$.

CYP24A1 is a member of the cytochrome P450 family, the main function of which is to convert 25 hydroxyvitamin D and $1\alpha,25(\text{OH})_2\text{D}_3$ to 24,25 hydroxyvitamin D and $1\alpha,24,25(\text{OH})_2\text{D}_3$, the inactive form of vitamin D (8). This process is a physiological protection to avoid the hypercalcemia that can be induced by high levels of $1\alpha,25(\text{OH})_2\text{D}_3$. It has been demonstrated that the expression of CYP24A1 is increased in prostate cancer and ovarian cancer cells after treatment with $1\alpha,25(\text{OH})_2\text{D}_3$ *in vitro* (15, 16). Other studies have shown that increasing levels of CYP24A1 reverse the anti-cancer effects of $1\alpha,25(\text{OH})_2\text{D}_3$ (17–19). Therefore, further investigation is needed to examine whether reduced CYP24A1 levels could enhance the anti-tumor efficacy of $1\alpha,25(\text{OH})_2\text{D}_3$ *via* suppressing EMT.

We have successfully built a spontaneous malignant transformation model of mouse OSE (MOSE) cells, and found that EMT was associated with the oncogenic transformation of MOSE cells. In the present study, We aimed to investigate whether $1\alpha,25(\text{OH})_2\text{D}_3$ could suppress the migration and invasion of MOSE cells during malignant transformation, and whether knockdown of CYP24A1 enhances the anti-cancer effects of $1\alpha,25(\text{OH})_2\text{D}_3$ by regulating EMT.

MATERIALS AND METHODS

MOSE Cell Isolation and Culture

MOSE cells were isolated using the method described by Roby et al. (20), and the model of spontaneous malignant transformation was established by our group (20). Briefly, single MOSE cells were collected from the ovaries of female C57BL/6 mice. Next, cells were cultured in Dulbecco's Modified Eagle's Medium/Nutrient Mixture F-12 (DMEM/F12, Invitrogen, Carlsbad, CA) culture media, supplemented with 20 ng/ml mEGF, 20 ng/ml mouse basic FGF, 2 $\mu\text{g}/\text{ml}$ insulin and 4 $\mu\text{g}/\text{ml}$ heparin sodium (Gibco, USA) in a humidified atmosphere of 5% CO₂ at 37°C. MOSE cells were continuously passaged *in vitro*. Over time, MOSE cells underwent spontaneous neoplastic transformation when subcultured for more than 80 passages *in vitro*. Based on morphological changes, chromosomal number, and proliferation ability, three sequential stages of transformed MOSE cells were defined as follows (data not published): early passage MOSE cells (M-E, ≤ 20 passages), intermediate-passage MOSE cells (M-I, 21–79 passages), and late-passage MOSE cells (M-L, ≥ 80 passages). The MOSE cells have been tested for mycoplasma and human cell lines contamination by STR profiling and were demonstrated to be clean (21). We did test the cytotoxicity of $1\alpha,25(\text{OH})_2\text{D}_3$ at doses of 1, 10, and 100 nM in three sequential stages of transformed MOSE cells, and found no significant inhibitory effects of $1\alpha,25(\text{OH})_2\text{D}_3$ on cell viability at the dose of 1 nM (**Supplementary Figure 1**). In this study, M-I and M-L cells were continuously treated with 1 nmol/L $1\alpha,25(\text{OH})_2\text{D}_3$ (Sigma, St. Louis, MO, USA).

Colony Formation and Soft Agar Colony Formation Assay

According to the previous protocol by Sun et al. (23), one thousands cells were seeded into a 6-well plates. The cells were cultured in a humidified incubator at 37°C with 5% CO₂ for 2 weeks. The medium was changed for every 3 days. The cell colonies were fixed with methanol for 15 min and stained with Giemsa's solution for 15 min, then washed with water and air-dried. The colonies with the diameter >0.5 mm were identified with ImageJ software. Plate colony formation efficiency was estimated by the number of clones divided by the number of cells inoculated. All experiments were repeated for 3 times and the average value was presented.

Cell suspensions were prepared as described above. A base layer of the mixture of 2 \times Ham's F-12 (Sigma Aldrich, 1/2) including 20% fetal bovine serum, and ultrapure LMP agarose (Sigma Aldrich, 1/2) was dissolved at 56°C for 20 min and then warmed to 37°C before the addition of top layer. A total of

2.5×10^4 cells were resuspended in $2 \times$ Ham's F-12 medium, and ultrapure LMP agarose, (1:1) and gently added onto the base layer. The cells were incubated at 37°C for 14 days, and 1 ml of fresh medium was added to the top layer every 3 days. Colonies were visualized using the EVOS XL imaging system (Life Technologies) and counted using ImageJ software.

Migration and Invasion Assays

The migration of MOSE cells was assessed using a wound healing assay. Cells were plated into a 6-well plate with FBS-free media for 12 h. Afterwards, cells cultured in the bottom of the well were scratched using a pipette tip to create a wound area. After 24 h, wounds (3 images each well) were imaged under a microscope ($\times 40$, CKX41F, Olympus, Tokyo, Japan) to detect the width of the gaps. Wound healing assay data is displayed as the migration index (%) = [(initial width)–(final width)]/(initial width). Values were normalized to the control group. Data points in the figure represent three independent experiments. For the detection of invasiveness, cells were seeded into Boyden Matrigel-coated chambers with $8\ \mu\text{m}$ pore inserts (BD Bioscience, San Jose, CA, USA). The lower chamber was supplemented with DMEM/ F12 media containing 10% FBS. After 24 h, the non-invasive cells were cleaned using a cotton swab. Then, cells at the bottom of the chamber were stained with crystal violet (c0121, Beyotime Biotechnology, Shanghai, China), and imaged under a microscope ($\times 400$, CKX41F, Olympus, Tokyo, Japan). The stained cells were then dissolved in 0.5 ml ethanol. Finally, OD values were obtained at 595 nm using a microplate reader (Molecular Devices, FiltorMax F5, USA).

Animal Experiments

Four to six weeks old (18–20 g) female BALB/C nude mice were purchased from the Shanghai Laboratory Animal Centre, Chinese Academy of Sciences, China. Animals were kept in a specific pathogen-free environment, with a temperature of $21 \pm 2^\circ\text{C}$, relative humidity of $55 \pm 5\%$ and a 12:12 h light-dark cycle. Mice were provided with water and food *ad libitum*. All surgical procedures and care provided to the animals were approved by the Institutional Animal Care and Use Committee of Soochow University (approval number is ECSU 201800049). A $200\ \mu\text{l}$ cell suspension containing 10^5 MOSE cells were injected intraperitoneally into mice. Ten mice were randomly assigned to vehicle (sesame oil with 2% ethanol) group ($N = 5$), and vitamin D3 (1,000 IU/week) treatment group ($N = 5$). Treatments were administered for 8 weeks. Body weight was monitored weekly. All mice were euthanized by cervical dislocation prior to tissue collection. The tumors were then dissected out and weighed. Tumor tissue was then fixed in formalin for 1 week. The tumors were dehydrated and cut into $4\ \mu\text{m}$ sections of paraffin-embedded tissue samples. The slices were then stained with hematoxylin and eosin (H&E).

Bioinformatic Data Analysis of GSE26903

GSE26903 data were retrieved from the National Center for Biotechnology Information's Gene Expression Omnibus (GEO) (<https://www.ncbi.nlm.nih.gov/geo/query/acc.cgi?acc=GSE26903>), which was microarray analysis result of gene

expressions in $1,25$ -dihydroxyvitamin D₃-treated ovarian cancer OVCAR3 cells. Raw data extraction and analysis were performed by the R software package (version 2.15, <http://www.r-project.org/>). For GSE26903, the edgeR package was used for DEG screening. P -value < 0.05 and absolute $\log_2\text{FC}$ bigger than 1 were used as the cut-off criteria based on Benjamini & Hochberg (BH) procedure. Intersect function in R was used for identifying DEGs. The Venn diagram was generated by VennDiagram R package.

Western Blotting

MOSE cells were lysed using RIPA buffer (P0013, Beyotime Biotechnology, Shanghai, China), and a BCA protein analysis kit (P0012, Beyotime Biotechnology, Shanghai, China) was used to determine protein concentration. Samples ($20\ \mu\text{g}$ protein per sample) were then separated by 10% SDS-PAGE (P0012A, Beyotime Biotechnology, Shanghai, China), followed by transfer to a polyvinylidene fluoride (PVDF) membrane (Millipore, Boston, MA, USA). Membranes were blocked with 5% skim milk and incubated overnight with primary antibodies at 4°C . Then, membranes were rinsed in Tween-20 phosphate buffer (PBST) three times, followed by incubation with secondary antibodies for 1 h at room temperature. Afterwards, membranes were washed three times in PBST. A chemiluminescent reagent (Millipore, Boston, MA, USA) was used to visualize the protein complexes. ImageJ was used to read the grayscale values (Integrated Optical Density, IOD). The relative expression level of targeted proteins relative to β -actin (the loading control) was then quantified. Data in figures represent at least three independent experiments. The following antibodies were acquired from Cell Signaling Technology (Irvine, CA, USA): E-cadherin (1:700, #5296), Vimentin (1:800, #5741), β -catenin (1:100, #9582), Snail (1:700, #3879), N-cadherin (1:700, #4061), β -actin (1:1,000, #3700), HRP-linked anti-rabbit IgG (1:2,000, #7074), HRP-linked anti-mouse IgG (1:2,000, #7076). CYP24A1 (1:500, ab203308) primary antibody was purchased from Abcam (Cambridge, MA, USA).

Immunofluorescence Staining

Twenty thousands MOSE cells were cultured on a glass cover slip (Thermo Fisher Scientific, Waltham, MA, USA), which was placed into 24-well plates. MOSE cells were treated with $1\alpha,25(\text{OH})_2\text{D}_3$ after cells had adhered to the cover slips. To prepare for immunostaining, cells were rinsed twice with fresh PBS, followed by fixing in 4% paraformaldehyde for 20 min. Then, 0.1% Triton was used to permeabilize cells at 4°C for 15 min, and nonspecific binding was blocked with 5% skim milk for 1 h at room temperature. Cells were then incubated with the following primary antibodies: E-cadherin (1:100), Snail (1:50) and β -catenin (1:100). Cells were then incubated with secondary antibody IgG-Cy5 (1:1,000, #4412, Cell Signaling Technology) for 1.5 h. Cell nuclei were labeled with DAPI. A confocal laser scanning microscope (TCS SP2, Leica, Wetzlar, Germany) was used to obtain fluorescent images.

RT-qPCR

Total RNA from MOSE cells was extracted with an RNeasy kit (Qiagen, Crawley, West Sussex, UK). The Transcriptor First

Strand cDNA Synthesis Kit (Roche, Mannheim, Germany) was then used to perform reverse transcription with 1 μg total RNA. Quantitative RT-PCR was performed to test the levels of CYP24A1 in MOSE cells and ascites cells, which were collected from mice injected with MOSE cells. The CYP24A1 primer set sequences were as follows: forward: 5'-CTGCCCATGACAA AAGGC-3'; reverse: 5'-CTCACCGTCGGTCATCAGC-3'. The β -actin primer set sequences were as follows: forward: 5'-GGCTGTATCCCCTCCATCG-3'; reverse: 5'-CCAGT TGGTAACAATGCCATGT-3'. The SYBR-Green I Nucleic Acid Gel stain (Roche) was applied to the qPCR. An ABI 7500 real-time PCR system was used to perform the RT-PCR reactions (Applied Biosystems, Foster City, CA, USA). Thermocycling parameters were: 95°C for 10 min, followed by 40 cycles of 95°C for 10 s, 60°C for 20 s and 72°C for 30 s. $2^{-\Delta\Delta C_t}$ method was used to calculate the relative expression levels (22). Six replicates for each sample were used for the calculations in each of the three independent experiments. The β -actin was used as an internal control.

Specific Lentiviral Knockdown of CYP24A1

CYP24A1 knockdown cells were produced by lentivirus infection. First, an online shRNA design tool MISSION[®] from Sigma-Aldrich was used to determine a set of top-scoring targets for CYP24A1. Then, shRNA oligo (5'-CCGGGCACAA TTTTCATAAACGCAAACCTCGAGTTTGCG TTTATGAAAT TGTGCTTTTTTG-3'), named as sh-CYP24A1, was synthesized for cloning into a PLKO.1 backbone. PLKO.1-scramble shRNA targeting no known genes from any species was used as a negative control, named as sh-NC (Sigma-Aldrich, SHC016). We then co-transfected psPAX2 and PLKO.1-shRNA plasmids into 293T cells. The pMD2.G plasmid was then enveloped and used to generate the sh-CYP24A1 lentivirus. The supernatant of 293T cells was collected after 48 h, and filtered using a 0.45 μm membrane. A mixture of lentivirus and media was combined with 5 ml media containing 8 mg/ml polybrene. MOSE cells were treated for 24 h with lentivirus-containing mixture followed by selection using puromycin (1 mg/ml) for an additional 48 h. Cells were then cultured for further analysis.

Statistical Analysis

Statistical analyses were performed using GraphPad Prism 7 (GraphPad Software Inc., La Jolla, CA, USA). Quantitative data are presented as the mean \pm standard deviation of the mean (SD). Statistical data were analyzed using a two-tailed, unpaired Student's *t*-test. $P < 0.05$ was considered statistically significant.

RESULTS

$1\alpha,25(\text{OH})_2\text{D}_3$ Partially Suppresses the Proliferation and Invasion of MOSE Cells Both *in vitro* and *in vivo*

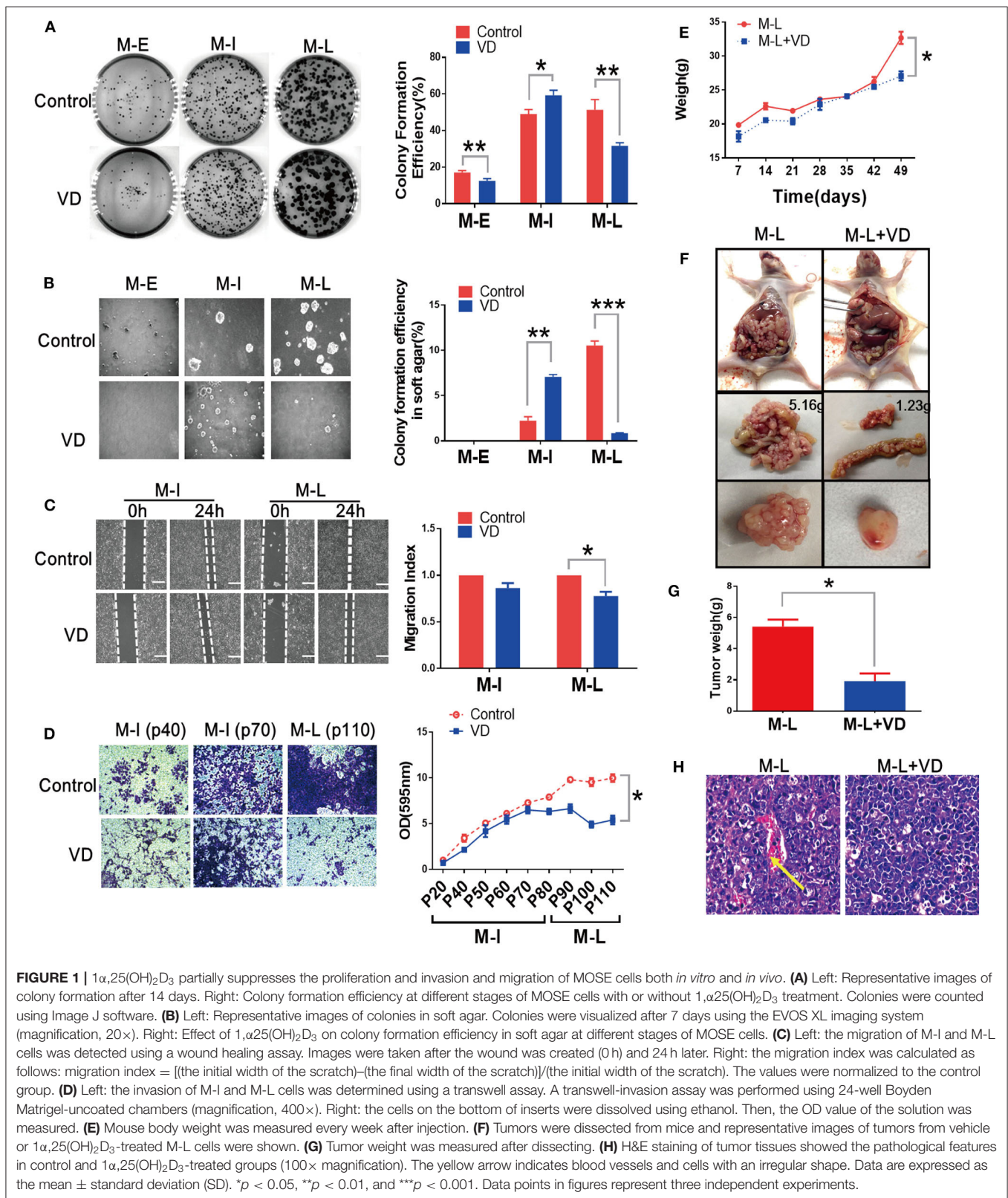
Previous study from our group has revealed that $1\alpha,25(\text{OH})_2\text{D}_3$ represses the migration of human ovarian cancer SKOV-3 cells (13). We wondered whether $1\alpha,25(\text{OH})_2\text{D}_3$ could hold back malignant transformation of MOSE cells. The MOSE cells were continually treated with $1\alpha,25(\text{OH})_2\text{D}_3$ from early (M-E),

intermediate (M-I) to late (M-L) passages. The colony formation efficiency in $1\alpha,25(\text{OH})_2\text{D}_3$ -treated M-E cells ($12.467 \pm 1.286\%$) was significantly lower than that of untreated M-E cells ($17.133 \pm 1.026\%$) ($p < 0.01$). And, $1\alpha,25(\text{OH})_2\text{D}_3$ significantly inhibited colony formation efficiency in M-L cells ($31.600 \pm 1.778\%$) compared with untreated M-L cells ($51.333 \pm 5.630\%$). However, $1,25(\text{OH})_2\text{D}_3$ -treated M-I cells exhibited significantly higher colony formation efficiency than the untreated cells ($p < 0.05$) (Figure 1A). Meanwhile, we observed that M-I and M-L, but not M-E cells, could form colonies in soft agar. $1\alpha,25(\text{OH})_2\text{D}_3$ -treatment significantly increased the colony formation efficiency of M-I cells in soft agar ($p < 0.01$), but it dramatically inhibited the colony formation efficiency of M-L cells ($p < 0.01$) (Figure 1B). As regard to migration, we found that there was no obvious difference in the migration index between the $1\alpha,25(\text{OH})_2\text{D}_3$ -treated group and the control group among M-I cells. However, $1\alpha,25(\text{OH})_2\text{D}_3$ significantly inhibited the migration of M-L cells compared with untreated cells ($p < 0.05$) (Figure 1C). Similarly, $1\alpha,25(\text{OH})_2\text{D}_3$ significantly decreased the invasion abilities of M-L cells, but it did not work in M-I cells ($p < 0.05$; Figure 1D). These results indicated that $1\alpha,25(\text{OH})_2\text{D}_3$ suppressed the proliferation and invasion of both M-E and M-L cells, but not in M-I cells.

Next, we determined the metastatic abilities of MOSE cells treated with or without $1\alpha,25(\text{OH})_2\text{D}_3$ *in vivo*. $1\alpha,25(\text{OH})_2\text{D}_3$ -treated or control MOSE cells were injected intraperitoneally into nude mice. We found that mice injected with M-I cells failed to form tumors, those injected with M-L cells produced tumors. As shown in Figure 1E, the body weights of mice injected with $1\alpha,25(\text{OH})_2\text{D}_3$ -treated M-L cells were significantly lower than the control group ($p < 0.05$). $1\alpha,25(\text{OH})_2\text{D}_3$ suppressed the metastasis of M-L cells compared to untreated-M-L cells *in vivo* (1.2335 vs. 5.1561 g). The ovarian tumors formed from $1\alpha,25(\text{OH})_2\text{D}_3$ -treated M-L cells were smaller than those from control M-L cells ($p < 0.05$, Figures 1F,G). H&E staining of tumor tissues showed that there were fewer irregularly shaped blood vessels and cells in the $1\alpha,25(\text{OH})_2\text{D}_3$ -treated group than in the corresponding control group (Figure 1H). These findings implied that $1\alpha,25(\text{OH})_2\text{D}_3$ dramatically inhibits the metastasis of M-L cells, yet has no effect on the M-I cells.

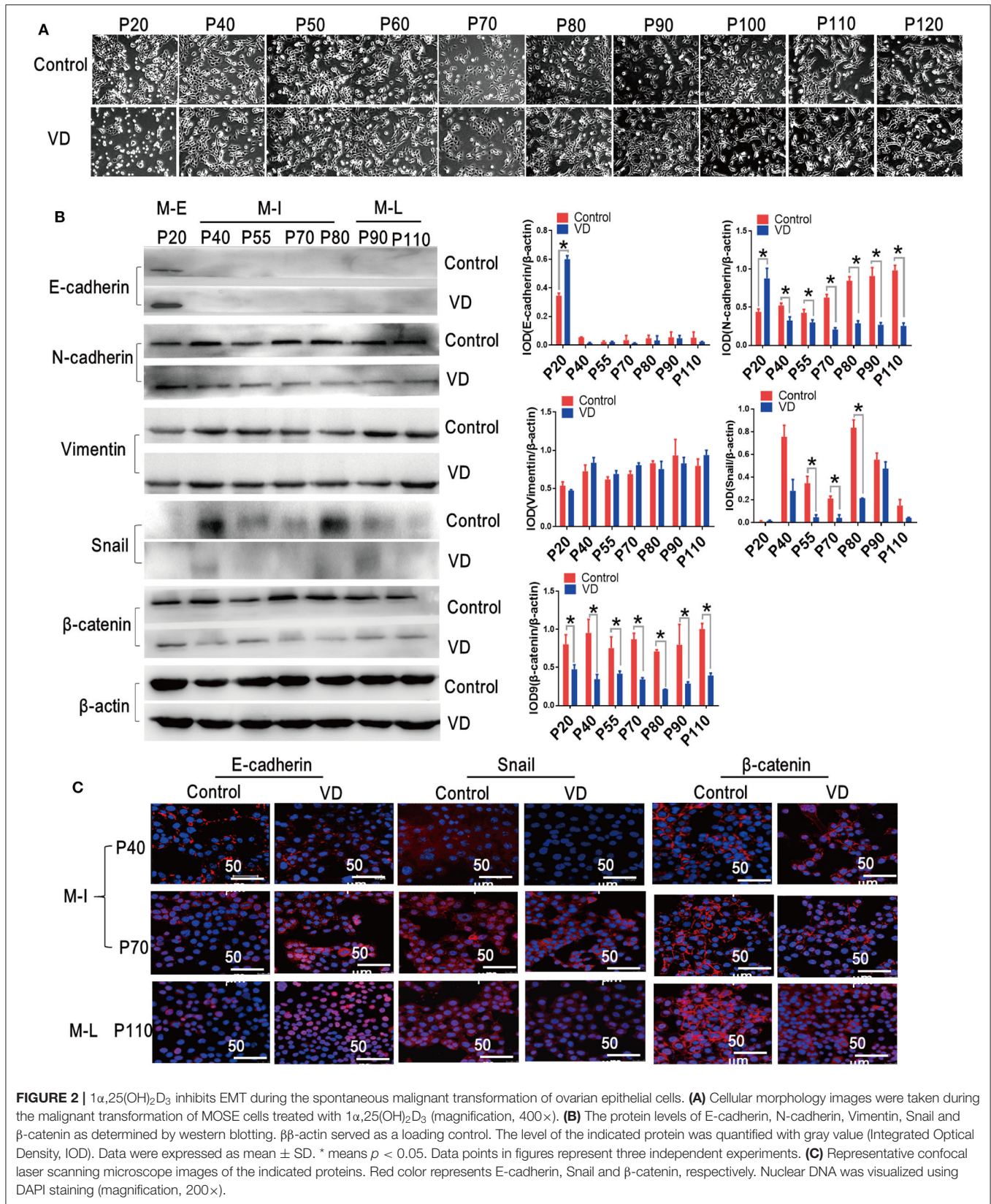
$1\alpha,25(\text{OH})_2\text{D}_3$ Inhibits EMT During Malignant Transformation of MOSE Cells

EMT plays an essential role in transforming epithelial cells into mesenchymal cells with more aggressive phenotype (23). Interestingly, we also observed that MOSE cells acquired a spindle-like shape during spontaneous malignant transformation, but this morphological change was blocked by $1\alpha,25(\text{OH})_2\text{D}_3$ (Figure 2A). To investigate whether $1\alpha,25(\text{OH})_2\text{D}_3$ inhibits EMT during the spontaneous malignant transformation of MOSE cells, we thus examined a series of EMT markers and transcription factors. We found that $1\alpha,25(\text{OH})_2\text{D}_3$ decreased the expression of N-cadherin in both M-I and M-L cells, compared with control cells ($p < 0.05$; Figure 2B). However, $1\alpha,25(\text{OH})_2\text{D}_3$ did not affect the



expression levels of E-cadherin, except in early cells (p20). Furthermore, $1\alpha,25(\text{OH})_2\text{D}_3$ significantly decreased the levels of Snail in M-I cells, and β -catenin in M-I and M-L cells

(Figure 2B). Immunofluorescence staining also revealed similar results, with the exception of E-cadherin (Figure 2C). Together, results from the morphological phenotype, invasion ability,



and protein expression patterns indicated that $1\alpha,25(\text{OH})_2\text{D}_3$ partially inhibited the EMT process.

Long-Term Treatment With $1\alpha,25(\text{OH})_2\text{D}_3$ Results in Elevated Levels of CYP24A1

To identify differentially expressed genes (DEGs) regulated by $1\alpha,25(\text{OH})_2\text{D}_3$ in inhibiting proliferation and invasion of ovarian cancer cells, we searched the microarray data of human ovarian adenocarcinoma OVCAR3 cells by the National Center for Biotechnology Information's Gene Expression Omnibus (GEO). The full set of raw data from this study was accessible from the link: <https://www.ncbi.nlm.nih.gov/geo/query/acc.cgi?acc=GSE26903>. Volcano plots were generated to visualize the distribution of DEGs between untreated and $1\alpha,25(\text{OH})_2\text{D}_3$ -treated OVCAR3 cells at 8, 24, and 72 h. Red or green dots in the plots represented significantly up-regulated or down-regulated genes, respectively (Figure 3A). Based on absolute $\log_2\text{FC} > 1$ cut-off criteria, total 61 were differentially expressed in common among three groups ($p < 0.05$). Among them, 40 genes were up-regulated and 21 were down-regulated (Figure 3B). In $1\alpha,25(\text{OH})_2\text{D}_3$ -treated OVCAR cells, CYP24A1 was the most up-regulated genes by 58-, 67-, and 69-fold increase after 8, 24, and 72 h treatment, respectively.

Rising levels of CYP24A1 induced by $1\alpha,25(\text{OH})_2\text{D}_3$ can antagonize the anti-metastatic effects of $1\alpha,25(\text{OH})_2\text{D}_3$ (16). To investigate whether the partial anti-metastatic effects of $1\alpha,25(\text{OH})_2\text{D}_3$ were associated with rising levels of CYP24A1, we measured CYP24A1 levels in M-E, M-I and M-L cells using qRT-PCR. The enhancements of CYP24A1 in M-I cells (>12,000-fold) was more obvious than M-E cells (370-fold) and M-L cells (1,600-fold) ($p < 0.0001$) (Figure 3C). The result from immunofluorescence staining also showed that the expression of CYP24A1 in M-I cells was more increased than that of other two cell lines. Additionally, CYP24A1 was diffusely located in the nuclei of M-I cells, but mainly expressed in the cytoplasm of M-E and M-L cells. On the contrary, CYP24A1 expression exhibited an opposite trend in $1\alpha,25(\text{OH})_2\text{D}_3$ -treated cells (Figure 3D). Similarly, there was a drastic increase in CYP24A1 expression (>15,000-fold) in ascites cells collected from mice injected with $1\alpha,25(\text{OH})_2\text{D}_3$ -treated M-L cells (Figure 3E). These findings demonstrate that the enhancement of CYP24A1 in M-I cells is higher than in M-L cells following $1\alpha,25(\text{OH})_2\text{D}_3$ treatment, which may be caused by the antagonism of CYP24A1 by $1\alpha,25(\text{OH})_2\text{D}_3$.

Knockdown of CYP24A1 Augments the Anti-Invasion Effects of $1\alpha,25(\text{OH})_2\text{D}_3$

Then, we sought to determine whether knockdown of CYP24A1 could enhance the anti-invasion properties of $1\alpha,25(\text{OH})_2\text{D}_3$. Figure 4A demonstrates the stable knockdown of CYP24A1 in M-I and M-L cells using the PLKO.1 lentiviral system. Although $1\alpha,25(\text{OH})_2\text{D}_3$ promoted the growth of sh-NC M-I cells, the knockdown of CYP24A1 meaningfully inhibited colony formation efficiency of both M-I and M-L cells treated by $1\alpha,25(\text{OH})_2\text{D}_3$ (Figure 4B), indicating that silencing CYP24A1 enhanced the effect of $1\alpha,25(\text{OH})_2\text{D}_3$ on inhibiting growth

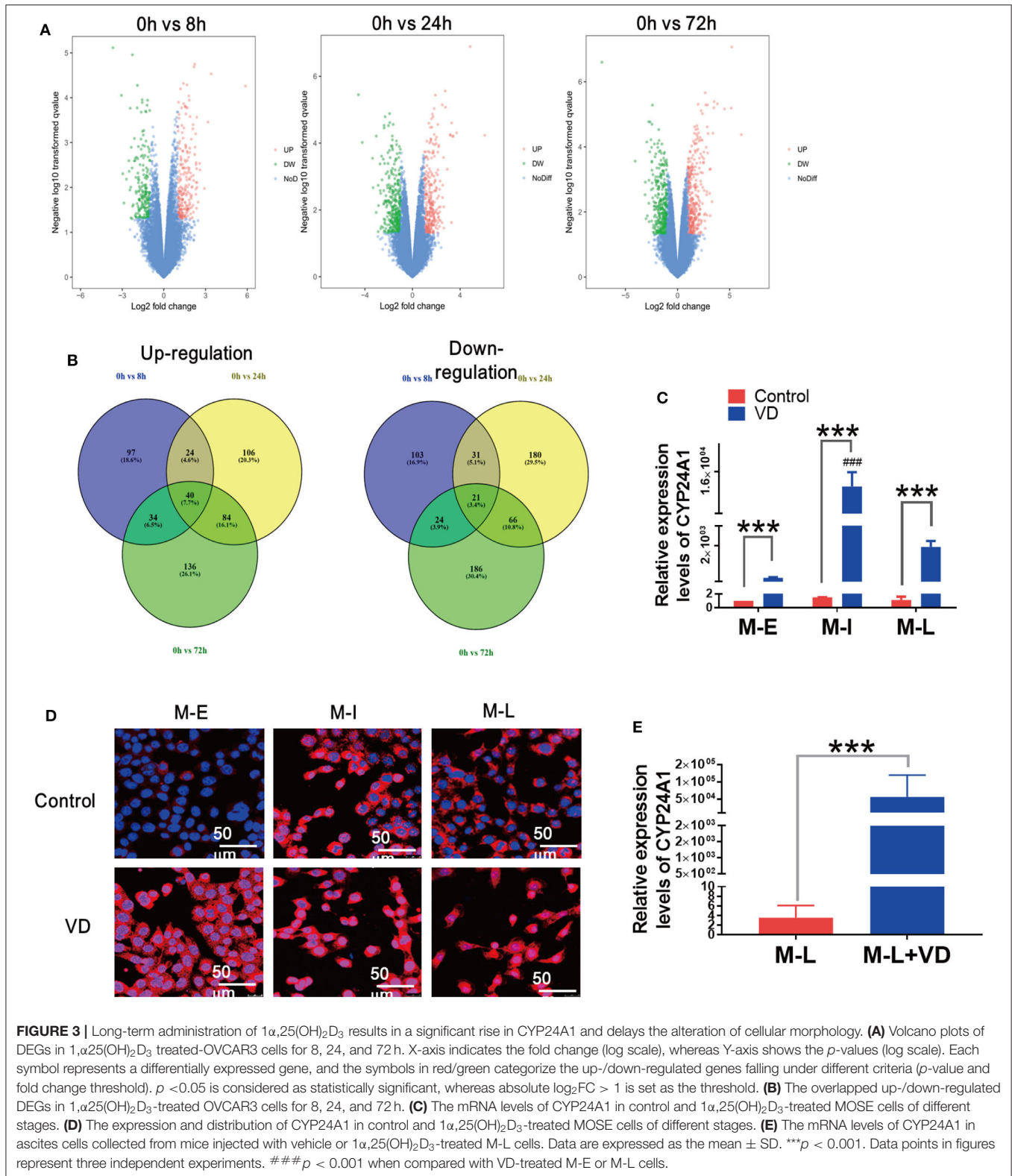
of MOSE cells. As demonstrated in Figure 4C, $1\alpha,25(\text{OH})_2\text{D}_3$ did not inhibit the migration of M-I cells transfected with sh-NC, but strongly inhibited the migration of sh-CYP24A1-transfected M-I cells. And it markedly reduced the migration of both NC and CYP24A1 knockdown M-L cells. Moreover, we found that the migration index in sh-CYP24A1-transfected M-I cells was lower than the sh-NC group, following treatment with $1\alpha,25(\text{OH})_2\text{D}_3$ ($p < 0.05$). Similarly, the invasion ability of CYP24A1 knockdown cells was weaker than that of sh-NC cells, in both M-I and M-L cells treated with $1\alpha,25(\text{OH})_2\text{D}_3$ ($p < 0.05$; Figure 4D). Subsequently, results from western blotting showed that only knockdown of CYP24A1 elevated the levels of E-cadherin in both M-I and M-L cells, not concerning $1\alpha,25(\text{OH})_2\text{D}_3$. $1\alpha,25(\text{OH})_2\text{D}_3$ increased the E-cadherin in sh-NC cells, but decreased that in shCYP24A1-transfected M-I and M-L cells. Further, $1\alpha,25(\text{OH})_2\text{D}_3$ reduced the expressions of N-cadherin, Vimentin, Snail and β -catenin significantly in both M-I and M-L cells with shCYP24A1 knockdown ($p < 0.05$, Figures 4E,F). These results further demonstrated that the loss of CYP24A1 increased the anti-invasion properties of $1\alpha,25(\text{OH})_2\text{D}_3$ by suppressing EMT.

DISCUSSION

Some evidence indicated that CYP24A1 overexpression resulted in cellular resistance to the antiproliferative effects of $1\alpha,25(\text{OH})_2\text{D}_3$ (8, 17, 24). The high levels of CYP24A1 also positively correlated with a poor outcome of cancers including ovarian, prostate, breast, thyroid, colorectal cancers and melanomas (14–18, 21). In this study, we found that $1\alpha,25(\text{OH})_2\text{D}_3$ significantly reduced the migration and invasion of malignant MOSE (M-L) cells by inhibiting EMT, yet had no effect on intermediate MOSE (M-I) cells. Interestingly, the levels of CYP24A1 in M-I cells were distinctly higher than in M-L cells following continuous treatment with $1\alpha,25(\text{OH})_2\text{D}_3$. Furthermore, we demonstrated that loss of CYP24A1 enhanced the anti-invasion properties of $1\alpha,25(\text{OH})_2\text{D}_3$ by suppressing EMT. These findings also imply that $1\alpha,25(\text{OH})_2\text{D}_3$ in combination with CYP24A1 inhibitor may have potential in the treatment of ovarian cancer.

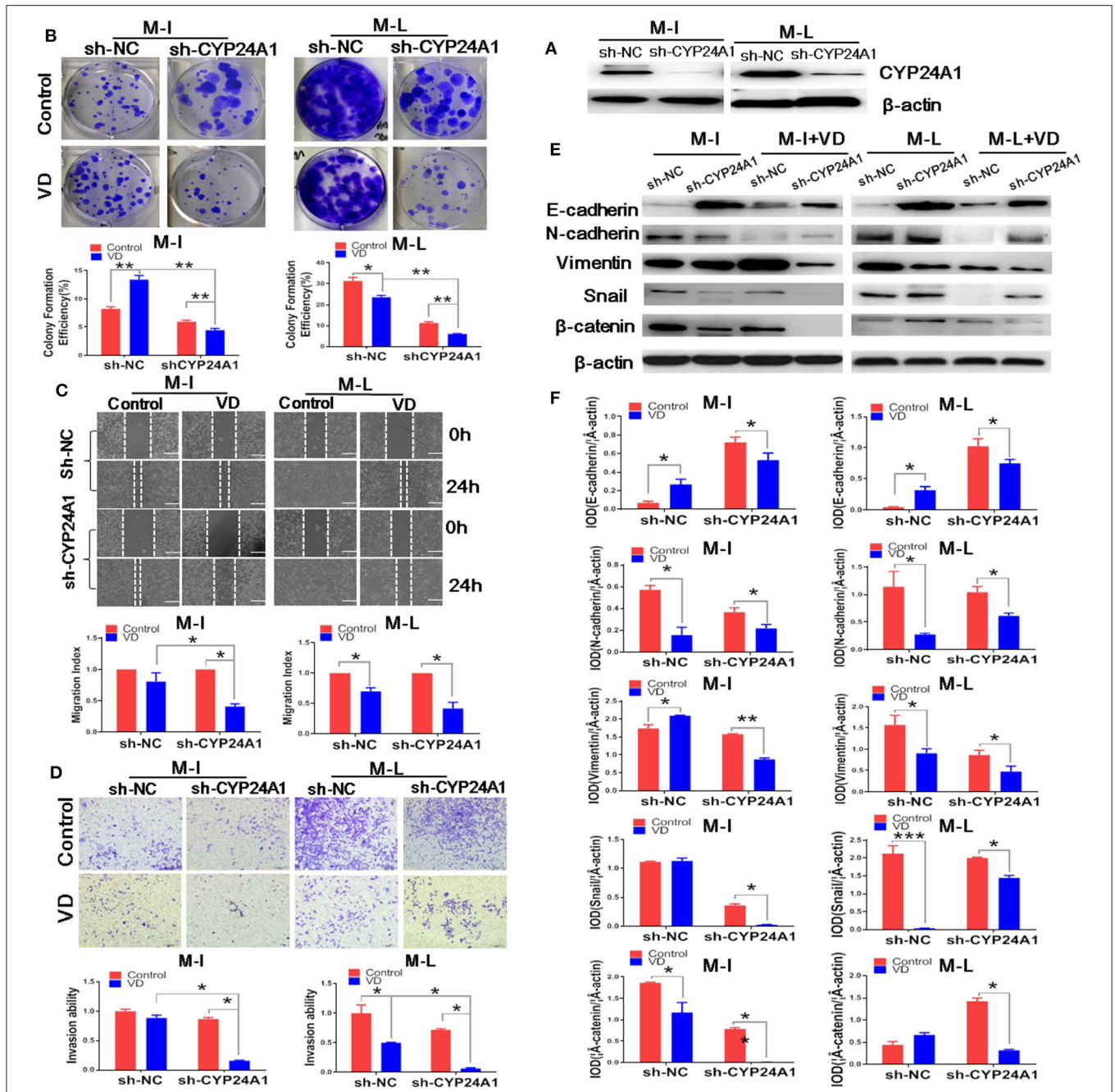
EMT is a process which can endow epithelial cells with increased capacity for invasiveness and mobility, giving them properties of mesenchymal cells (23). In most cases, EMT plays not only an essential role in embryonic development but also serves an important biological function in normal OSE cells. The EMT of OSE cells in response to postovulatory stimuli has been thought to enhance their postovulatory repair (25). However, abnormalities in the EMT process resulted in the uncontrolled proliferation of OSE cells, which may lead to tumorigenesis (26). Moreover, many reports have shown that EMT is relevant to dissemination and metastasis of ovarian cancer (27–29).

There are several different ways by which $1\alpha,25(\text{OH})_2\text{D}_3$ exerts anti-tumor effects, including the induction of cellular apoptosis and differentiation, and the inhibition of proliferation and angiogenesis (9). Moreover, $1\alpha,25(\text{OH})_2\text{D}_3$ has been shown to repress the migration and invasion abilities of multiple types



of cancer cells, including prostate cancer (30), breast cancer (31), and pancreatic cancer (32). $1\alpha,25(\text{OH})_2\text{D}_3$ and its synthetic derivatives also have anti-cancer effects in animal models (10,

33, 34). Briefly, the results of some studies have indicated that $1\alpha,25(\text{OH})_2\text{D}_3$ decreases the migration and invasion of malignant tumor cells by suppressing EMT (10–13, 35). It has



also been reported that $1\alpha,25(\text{OH})_2\text{D}_3$ suppresses the migration of ovarian cancer (12), lung cancer (35) and colon cancer cells (10) through repressing TGF- β 1-induced EMT. In this study, we found that $1\alpha,25(\text{OH})_2\text{D}_3$ represses EMT by inhibiting β -catenin, N-cadherin and Snail expressions in malignant M-L cells. However, $1\alpha,25(\text{OH})_2\text{D}_3$ showed no effect on E-cadherin in M-I or M-L cells, and it reduced the E-cadherin expressions when CYP24A1 was knocked-down. The recent study revealed that E-cadherin functions as a survival factor in invasive breast cancer during nearly all phases of metastasis, which hints strategy to inhibit E-cadherin-mediated survival may have potential as a therapeutic approach (36). Meanwhile, another research reported that $1\alpha,25(\text{OH})_2\text{D}_3$ is efficient in countering EMT phenotype only when combined with TGF- β , but not at a later stage (37). Thus, it is worth to explore why $1\alpha,25(\text{OH})_2\text{D}_3$ decreased the of E-cadherin expression while it inhibited the invasion of ovarian cancer cells.

Although $1\alpha,25(\text{OH})_2\text{D}_3$ reduced the expression of N-cadherin, Snail and β -catenin in intermediate transformation (M-I) cells, it was unable to decrease their migration and invasion properties. We found that the expression of CYP24A1 in M-I cells was dramatically higher than that in M-L cells following $1\alpha,25(\text{OH})_2\text{D}_3$ treatment. Previous research has also revealed aberrantly high levels of CYP24A1 in multiple kinds of cancer cells, including ovarian cancer, breast cancer, thyroid cancer, and glioma cells (38–41), thereby making them resistant to $1\alpha,25(\text{OH})_2\text{D}_3$. Loss of CYP24A1 therefore facilitated the anti-tumor efficacy of $1\alpha,25(\text{OH})_2\text{D}_3$ in lung (42), colorectal (19), endometrial (43) and thyroid cancer cells (17). These studies further revealed that knockdown of CYP24A1 repressed the Wnt/ β -catenin and Akt signaling pathways. In the present study, we found that $1\alpha,25(\text{OH})_2\text{D}_3$ only restricted the migration and invasion abilities of M-L cells but not M-I cells, which may be owing to the higher CYP24A1 expression levels in M-I cells. After knockdown of CYP24A1, $1\alpha,25(\text{OH})_2\text{D}_3$ dramatically suppressed the migration and invasion in both M-I and M-L cells. Furthermore, $1\alpha,25(\text{OH})_2\text{D}_3$ decreased the expressions of Vimentin, N-cadherin, β -catenin and Snail in both M-I and M-L cells with stable knockdown of CYP24A1. These results are consistent with a previous finding that CYP24A1 depletion augments the suppressive ability of $1\alpha,25(\text{OH})_2\text{D}_3$ on EMT (17).

The other important finding of this study emerges from the phenomenon that knockdown of CYP24A1 increased the levels of E-cadherin in both M-I and M-L cells, and reduced Vimentin (M-L), N-cadherin (M-I), β -catenin (M-L) and Snail (M-I), hinting that silencing CYP24A1 could inhibit EMT. In fact, our results are in agreements with the data described in recent studies

(39–41, 44), which suggest CYP24A1 as a potential oncogene. Therefore, it is worth noting whether CYP24A1 would play an oncogenic role through regulating EMT.

In summary, $1\alpha,25(\text{OH})_2\text{D}_3$ partially suppresses the proliferation and invasion of malignant ovarian cancer cells *in vitro* and *in vivo* by inhibiting EMT. Moreover, loss of CYP24A1 not only promotes the inhibitory effects of $1\alpha,25(\text{OH})_2\text{D}_3$ on the migration and invasiveness of intermediately transformed and malignant ovarian cancer cells by inhibiting EMT, but also directly suppresses EMT. These findings provide research foundation for making CYP24A1 a potential target to activate the vitamin D pathway in the treatment of ovarian cancer.

DATA AVAILABILITY STATEMENT

The datasets presented in this study can be found in online repositories. The names of the repository/repositories and accession number(s) can be found in the article/**Supplementary Material**.

ETHICS STATEMENT

The animal study was reviewed and approved by Institutional Animal Care and Use Committee of Soochow University.

AUTHOR CONTRIBUTIONS

PW, JX, WY, and YH finished the experiments and data analysis. PW and BL designed the experiments. JX, PW, and WH wrote the manuscript and the manuscript was reviewed by BL and ZZ. The funding was acquired by BL, PW, and WH. All authors contributed to the article and approved the submitted version.

ACKNOWLEDGMENTS

The authors wish to acknowledge the supports of the National Natural Scientific Funding of China (grants 81673151, 81703225, and 81872622). This research was funded by the State Key Laboratory of Radiation Medicine and Protection, Medical College of Soochow University, Collaborative Innovation Center of Radiation Medicine of Jiangsu Higher Education Institution.

SUPPLEMENTARY MATERIAL

The Supplementary Material for this article can be found online at: <https://www.frontiersin.org/articles/10.3389/fonc.2020.01258/full#supplementary-material>

REFERENCES

- Dongre A, Weinberg RA. New insights into the mechanisms of epithelial-mesenchymal transition and implications for cancer. *Nat Rev Mol Cell Biol.* (2019) 20:69–84. doi: 10.1038/s41580-018-0080-4
- Vergara D, Merlot B, Lucot JP, Collinet P, Vinatier D, Fournier I, et al. Epithelial-mesenchymal transition in ovarian cancer. *Cancer Lett.* (2010) 291:59–66. doi: 10.1016/j.canlet.2009.09.017
- Ocana OH, Corcoles R, Fabra A, Moreno-Bueno G, Aclaque H, Vega S, et al. Metastatic colonization requires the repression of the epithelial-mesenchymal transition inducer Prrx1. *Cancer Cell.* (2012) 22:709–24. doi: 10.1016/j.ccr.2012.10.012
- Kiesslich T, Pichler M, Neureiter D. Epigenetic control of epithelial-mesenchymal-transition in human cancer. *Mol Clin Oncol.* (2013) 1:3–11. doi: 10.3892/mco.2012.28

5. Meng F, Wu G. The rejuvenated scenario of epithelial-mesenchymal transition (EMT) and cancer metastasis. *Cancer Metastasis Rev.* (2012) 31:455–67. doi: 10.1007/s10555-012-9379-3
6. Shang Y, Cai X, Fan D. Roles of epithelial-mesenchymal transition in cancer drug resistance. *Curr Cancer Drug Targets.* (2013) 13:915–29. doi: 10.2174/15680096113136660097
7. Bonnomet A, Syne L, Brysse A, Feyereisen E, Thompson EW, Noel A, et al. A dynamic *in vivo* model of epithelial-to-mesenchymal transitions in circulating tumor cells and metastases of breast cancer. *Oncogene.* (2012) 31:3741–53. doi: 10.1038/ncr.2011.540
8. Deeb KK, Trump DL, Johnson CS. Vitamin D signalling pathways in cancer: potential for anticancer therapeutics. *Nat Rev Cancer.* (2007) 7:684–700. doi: 10.1038/nrc2196
9. Feldman D, Krishnan AV, Swami S, Giovannucci E, Feldman BJ. The role of vitamin D in reducing cancer risk and progression. *Nat Rev Cancer.* (2014) 14:342–57. doi: 10.1038/nrc3691
10. Chen S, Zhu J, Zuo S, Ma J, Zhang J, Chen G, et al. 1,25(OH) $_2$ D $_3$ attenuates TGF-beta1/beta2-induced increased migration and invasion via inhibiting epithelial-mesenchymal transition in colon cancer cells. *Biochem Biophys Res Commun.* (2015) 468:130–5. doi: 10.1016/j.bbrc.2015.10.146
11. Chiang KC, Chen SC, Yeh CN, Pang JH, Shen SC, Hsu JT, et al. MART-10, a less calcemic vitamin D analog, is more potent than 1 α ,25-dihydroxyvitamin D $_3$ in inhibiting the metastatic potential of MCF-7 breast cancer cells *in vitro*. *J Steroid Biochem Mol Biol.* (2014) 139:54–60. doi: 10.1016/j.jsbmb.2013.10.005
12. Chiang KC, Yeh CN, Hsu JT, Jan YY, Chen LW, Kuo SF, et al. The vitamin D analog, MART-10, represses metastasis potential via downregulation of epithelial-mesenchymal transition in pancreatic cancer cells. *Cancer Lett.* (2014) 354:235–44. doi: 10.1016/j.canlet.2014.08.019
13. Hou YF, Gao SH, Wang P, Zhang HM, Liu LZ, Ye MX, et al. 1 α ,25(OH) $_2$ (D) $_3$ suppresses the migration of ovarian cancer SKOV-3 cells through the inhibition of epithelial-mesenchymal transition. *Int J Mol Sci.* (2016) 17:1285 doi: 10.3390/ijms17081285
14. Prescott J, Bertrand KA, Poole EM, Rosner BA, Tworoger SS. Surrogates of long-term vitamin d exposure and ovarian cancer risk in two prospective cohort studies. *Cancers.* (2013) 5:1577–600. doi: 10.3390/cancers5041577
15. Miettinen S, Ahonen MH, Lou YR, Manninen T, Tuohimaa P, Syvala H, et al. Role of 24-hydroxylase in vitamin D $_3$ growth response of OVCAR-3 ovarian cancer cells. *Int J Cancer.* (2004) 108:367–73. doi: 10.1002/ijc.11520
16. Tannour-Louet M, Lewis SK, Louet JF, Stewart J, Addai JB, Sahin A, et al. Increased expression of CYP24A1 correlates with advanced stages of prostate cancer and can cause resistance to vitamin D $_3$ -based therapies. *FASEB J.* (2014) 28:364–72. doi: 10.1096/fj.13-236109
17. Hu N, Zhang H. CYP24A1 depletion facilitates the antitumor effect of vitamin D $_3$ on thyroid cancer cells. *Exp Ther Med.* (2018) 16:2821–30. doi: 10.3892/etm.2018.6536
18. Osanai M, Lee GH. CYP24A1-induced vitamin D insufficiency promotes breast cancer growth. *Oncol Rep.* (2016) 36:2755–62. doi: 10.3892/or.2016.5072
19. Sun H, Jiang C, Cong L, Wu N, Wang X, Hao M, et al. CYP24A1 inhibition facilitates the antiproliferative effect of 1,25(OH) $_2$ D $_3$ through downregulation of the WNT/beta-catenin pathway and methylation-mediated regulation of CYP24A1 in colorectal cancer cells. *DNA Cell Biol.* (2018) 37:742–9. doi: 10.1089/dna.2017.4058
20. Gamwell LF, Collins O, Vanderhyden BC. The mouse ovarian surface epithelium contains a population of LY6A (SCA-1) expressing progenitor cells that are regulated by ovulation-associated factors. *Biol Reprod.* (2012) 87:80. doi: 10.1095/biolreprod.112.100347
21. Ji MT, Liu LZ, Hou YF, Li BY. 1 α ,25-Dihydroxyvitamin D $_3$ restrains stem cell-like properties of ovarian cancer cells by enhancing vitamin D receptor and suppressing CD44. *Oncol Rep.* (2019) 41:3393–403. doi: 10.3892/or.2019.7116
22. Livak KJ, Schmittgen TD. Analysis of relative gene expression data using real-time quantitative PCR and the 2(-Delta Delta C(T)) method. *Methods.* (2001) 25:402–8. doi: 10.1006/meth.2001.1262
23. Kalluri R, Weinberg RA. The basics of epithelial-mesenchymal transition. *J Clin Invest.* (2009) 119:1420–8. doi: 10.1172/JCI39104
24. Luo W, Yu WD, Ma Y, Chernov M, Trump DL, Johnson CS. Inhibition of protein kinase CK2 reduces Cyp24a1 expression and enhances 1,25-dihydroxyvitamin D(3) antitumor activity in human prostate cancer cells. *Cancer Res.* (2013) 73:2289–97. doi: 10.1158/0008-5472.CAN-12-4119
25. Ahmed N, Thompson EW, Quinn MA. Epithelial-mesenchymal interconversions in normal ovarian surface epithelium and ovarian carcinomas: an exception to the norm. *J Cell Physiol.* (2007) 213:581–8. doi: 10.1002/jcp.21240
26. Larriba MJ, Garcia de Herreros A, Munoz A. Vitamin D and the epithelial to mesenchymal transition. *Stem Cells Int.* (2016) 2016:6213872. doi: 10.1155/2016/6213872
27. Davidson B, Trope CG, Reich R. Epithelial-mesenchymal transition in ovarian carcinoma. *Front Oncol.* (2012) 2:33. doi: 10.3389/fonc.2012.00033
28. Li D, Pan Y, Huang Y, Zhang P, Fang X. PAK5 induces EMT and promotes cell migration and invasion by activating the PI3K/AKT pathway in ovarian cancer. *Anal Cell Pathol.* (2018) 2018:8073124. doi: 10.1155/2018/8073124
29. Mu Y, Li N, Cui YL. The lncRNA CCAT1 upregulates TGFbetaR1 via sponging miR-490-3p to promote TGFbeta1-induced EMT of ovarian cancer cells. *Cancer Cell Int.* (2018) 18:145. doi: 10.1186/s12935-018-0604-1
30. Sung V, Feldman D. 1,25-Dihydroxyvitamin D $_3$ decreases human prostate cancer cell adhesion and migration. *Mol Cell Endocrinol.* (2000) 164:133–43. doi: 10.1016/S0303-7207(00)00226-4
31. Colston KW, Lowe LC, Mansi JL, Campbell MJ. Vitamin D status and breast cancer risk. *Anticancer Res.* (2006) 26:2573–80. Available online at: <http://ar.iiarjournals.org/content/26/4A/2573.long>
32. Chiang KC, Chen TC. Vitamin D for the prevention and treatment of pancreatic cancer. *World J Gastroenterol.* (2009) 15:3349–54. doi: 10.3748/wjg.15.3349
33. Kawar N, Maclaughlan S, Horan TC, Uzun A, Lange TS, Kim KK, et al., PT19c, another nonhypercalcemic vitamin D $_2$ derivative, demonstrates antitumor efficacy in epithelial ovarian and endometrial cancer models. *Genes Cancer.* (2013) 4:524–34. doi: 10.1177/1947601913507575
34. Lange TS, Stuckey AR, Robison K, Kim KK, Singh RK, Raker CA, et al. Effect of a vitamin D(3) derivative (B3CD) with postulated anti-cancer activity in an ovarian cancer animal model. *Invest New Drugs.* (2010) 28:543–53. doi: 10.1007/s10637-009-9284-y
35. Upadhyay SK, Verone A, Shoemaker S, Qin M, Liu S, Campbell M, et al. 1,25-Dihydroxyvitamin D $_3$ (1,25(OH) $_2$ D $_3$) signaling capacity and the epithelial-mesenchymal transition in non-small cell lung cancer (NSCLC): implications for use of 1,25(OH) $_2$ D $_3$ in NSCLC treatment. *Cancers.* (2013) 5:1504–21. doi: 10.3390/cancers5041504
36. Padmanaban V, Krol I, Suhail Y, Szczerba BM, Aceto N, Bader JS, et al. E-cadherin is required for metastasis in multiple models of breast cancer. *Nature.* (2019) 573:439–44. doi: 10.1038/s41586-019-1526-3
37. Ricca C, Aillon A, Viano M, Bergandi L, Aldieri E, Silvagno F. Vitamin D inhibits the epithelial-mesenchymal transition by a negative feedback regulation of TGF-beta activity. *J Steroid Biochem Mol Biol.* (2019) 187:97–105. doi: 10.1016/j.jsbmb.2018.11.006
38. Friedrich M, Rafi L, Mitschele T, Tilgen W, Schmidt W, Reichrath J. Analysis of the vitamin D system in cervical carcinomas, breast cancer and ovarian cancer. *Recent Results Cancer Res.* (2003) 164:239–46. doi: 10.1007/978-3-642-55580-0_17
39. Sheng L, Turner AG, Barratt K, Kremer R, Morris HA, Callen DE, et al. Mammary-specific ablation of Cyp24a1 inhibits development, reduces proliferation and increases sensitivity to vitamin D. *J Steroid Biochem Mol Biol.* (2019) 56:65–73. doi: 10.1016/j.jsbmb.2019.01.005
40. Zou M, Baitei EY, BinEssa HA, Al-Mohanna FA, Parhar RS, St-Arnaud R, et al. Cyp24a1 attenuation limits progression of braf(V600E)-induced papillary thyroid cancer cells and sensitizes them to BRAF(V600E) inhibitor PLX4720. *Cancer Res.* (2017) 77:2161–72. doi: 10.1158/0008-5472.CAN-16-2066

41. Hu P, Li S, Tian N, Wu F, Hu Y, Li D, et al. Acidosis enhances the self-renewal and mitochondrial respiration of stem cell-like glioma cells through CYP24A1-mediated reduction of vitamin D. *Cell Death Dis.* (2019) 10:25. doi: 10.1038/s41419-018-1242-1
42. Shiratsuchi H, Wang Z, Chen G, Ray P, Lin J, Zhang Z, et al. Oncogenic potential of CYP24A1 in lung adenocarcinoma. *J Thorac Oncol.* (2017) 12:269–80. doi: 10.1016/j.jtho.2016.10.010
43. Bokhari AA, Lee LR, Raboteau D, Turbov J, Rodriguez IV, Pike JW, et al. Progesterone potentiates the growth inhibitory effects of calcitriol in endometrial cancer via suppression of CYP24A1. *Oncotarget.* (2016) 7:77576–90. doi: 10.18632/oncotarget.12725
44. Albertson DG, Ylstra B, Segraves R, Collins C, Dairkee SH, Kowbel D, et al. Quantitative mapping of amplicon structure by array CGH identifies

CYP24 as a candidate oncogene. *Nat Genet.* (2000) 25:144–6. doi: 10.1038/75985

Conflict of Interest: The authors declare that the research was conducted in the absence of any commercial or financial relationships that could be construed as a potential conflict of interest.

Copyright © 2020 Wang, Xu, You, Hou, Wang, Ma, Tan, Zhang, Hu and Li. This is an open-access article distributed under the terms of the Creative Commons Attribution License (CC BY). The use, distribution or reproduction in other forums is permitted, provided the original author(s) and the copyright owner(s) are credited and that the original publication in this journal is cited, in accordance with accepted academic practice. No use, distribution or reproduction is permitted which does not comply with these terms.